

Influence of Flux on the Structural and Thermoluminescence Properties of $Y_2SiO_5:Dy^{3+}$ Nanophosphors for Dosimetric Applications

K. DHANALAKSHMI^{1,*}, A. JAGANNATHA REDDY² and V. REVATHI¹

¹Department of Physics, New Horizon College of Engineering, Bangalore-560103, India

²Department of Physics, M.S. Ramaiah Institute of Technology, Bangalore-560054, India

*Corresponding author: E-mail: dhanalakshmi.kurakula@gmail.com

Received: 6 August 2021;

Accepted: 9 March 2022;

Published online: 20 April 2022;

AJC-20784

Potassium nitrate (KNO_3) and ammonium chloride (NH_4Cl) flux were added during the combustion synthesis of $Y_2SiO_5:Dy^{3+}$ (9 mol %) nanophosphors, which influenced its structure, morphology and thermoluminescent properties. Reduction in the crystallite size to ~ 7 nm observed using XRD analysis. Surface morphology enhanced in terms of its texture. Thermoluminescence analysis of the prepared phosphors irradiated with gamma dose over a range of 500 Gy – 4 KGy at a constant heating rate $3\text{ }^\circ\text{C s}^{-1}$ have been carried out. Kinetic parameters were evaluated by Chens method and activation energy was found to be 1.01-1.3 eV. Flux addition resulted in creation of large number of charge carriers and hence the material become the potential for dosimetry applications.

Keywords: Yttrium silicate, Potassium nitrate, Ammonium chloride, Thermoluminescence, Dosimetry, Flux effect.

INTRODUCTION

Commercial thermoluminescence detectors (TLDs) are in the form of crystalline materials. Phosphors after exposure to γ -radiations traps electron and whole pairs in the bandgap. Irradiated samples, when exposed with constant heating rate emits trapped electrons [1]. Thermally stimulated luminescence is a thermoluminescence, which is an emission of luminescence from a material consequent the absorption of energy from an external source by that material [2]. Thermoluminescence (TL) materials are used for different applications such as personal dosimetry, environmental dosimetry, TLD badges, etc. For these applications, researchers are exploring novel materials, which are suitable as a TLD material over a broad variety of irradiation.

The core problem of TL dosimeter made of $LiF:Mg,Cu,P$ or $Al_2O_3:C$, is the reduction in the response of these materials with increasing dose. The bandgap in yttrium silicate (Y_2SiO_5) is wide with defects present in it will impact the electrical and optical properties in the material which are controlled by charge carriers and excitons [3].

Y_2SiO_5 is proved to be a promising candidate for dosimetry applications. As reported in previous articles such as Sm^{3+}

doped Y_2SiO_5 [4], Dy^{3+} doped Y_2SiO_5 [5] Ce^{3+} doped Y_2SiO_5 [6] are recorded. Some of the works reported on Eu^{3+} doped Y_2SiO_5 phosphor [7], Ce^{3+} doped Y_2SiO_5 [8], phase dependent Sm^{3+} doped Y_2SiO_5 [9] and its effect of different fuels on thermoluminescence properties of Y_2SiO_5 are also studied [10].

In this work, we demonstrated that potassium nitrate and ammonium chloride fluxes addition influences the crystallite parameters, morphology and thermoluminescence properties, which in turn can be useful for TLD applications.

EXPERIMENTAL

Synthesis: For the synthesis of phosphors using combustion method [10,11], 0.027 g of Dy_2O_3 and 1.109 g of Y_2O_3 were taken initially as raw materials to which 1:1 HNO_3 was added. This aqueous solution was kept over a sand bath and heated to remove the surplus HNO_3 . To this transparent solution, 0.3 g of SiO_2 , 0.04308 g of KNO_3 and 1.77 g of ODH were added. This mixture is kept in muffle furnace at a temperature of ~ 500 $^\circ\text{C}$, which undergoes combustion reaction. The obtained product was calcined at 1300 $^\circ\text{C}$ for 3 h. Similar procedure was followed to prepare another sample using 0.04308 g of NH_4Cl flux.

RESULTS AND DISCUSSION

Phase identification of $Y_2SiO_5:Dy^{3+}$ doped with various flux: Phase purity of synthesized samples were studied by XRD analysis. Fig. 1 illustrates the XRD structures of samples were made using both KNO_3 and NH_4Cl fluxes [JCPDS card number 36-1476]. The diffraction patterns are stable with the standard data indicating that prepared phosphors are matching with pure monoclinic phase of Y_2SiO_5 [10].

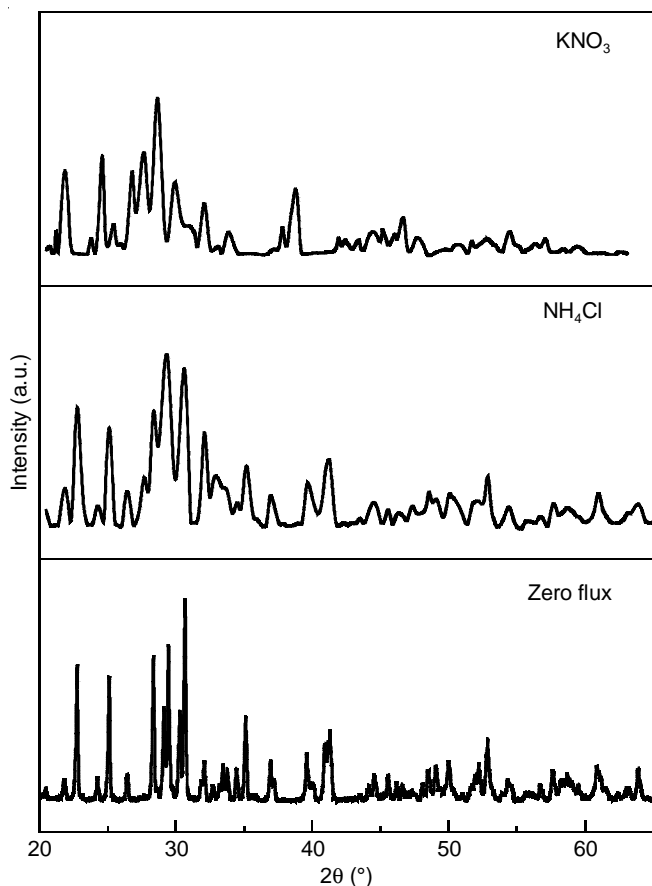


Fig. 1. PXRD patterns of different fluxes used in $Y_2SiO_5:Dy^{3+}$ (9 mol %) nanophosphor

Addition of fluxes results in lower phase transformation as flux has decomposition reaction at quite lower temperature

[12]. Moreover, no additional flux diffraction peaks were observed in the XRD pattern inferring that there exists ignorable effect on the unpurified samples. Similarly in the flux KNO_3 sample, there exists a small shift in the peak. The flux KNO_3 doped into Y_2SiO_5 matrix causes expansion of the unit cell resulting in tensile stress, as a result the PXRD peaks shifted towards lower angle side [13]. The crystallite size (D) for the flux was estimated by Scherrer's relation given by the eqn. 1:

$$D = \frac{K\lambda}{\beta \cos \theta} \quad (1)$$

As in eqn. 1, ' λ ' represents the wavelength of X-ray (1.542 Å), the Bragg angle ' θ ', ' K ' denotes the constant depends on the shape of the grain (0.94 for spherical). It is obvious that for zero flux since the diffraction peaks are narrowly broad, the crystallite size is estimated to be 65 nm. The effect of fluxes on this host influences the broadening of the peaks and hence it results small crystallite size ~ 22 nm.

FT-IR analysis: FT-IR spectra of the zero flux, NH_4Cl and KNO_3 used in $Y_2SiO_5:Dy^{3+}$ (9 mol %) nanophosphors recorded are shown in Fig. 2. For zero flux, the bands at 593 cm^{-1} can be attributed to stretching vibrations of Y-O bonds and the bands $> 800\text{ cm}^{-1}$ can be attributed to the Si-O bands. Similarly, for NH_4Cl added sample, the bands at 599 cm^{-1} are attributed to Y-O stretching bands, while the bands at 841 cm^{-1} and 881 cm^{-1} are the characteristic of M-O bands. The bands above 900 cm^{-1} are due to the Si-O vibrations. Furthermore, for KNO_3 the bands at $461, 511, 532, 548$ and 585 cm^{-1} are attributed to Y-O stretching vibrations. The bands at $875, 715$ and 686 cm^{-1} are due to the M-O bonds. The bands above 800 cm^{-1} are the characteristics of Si-O bonds [14].

SEM & EDAX: Morphological studies of the prepared phosphors were examined by scanning electron microscopy (SEM) technique. The SEM micrographs in Fig. 3a, Fig. 4a and Fig. 5a were recorded for samples with zero flux (magnification 45 kx), NH_4Cl (magnification 40 kx), KNO_3 (magnification 40 kx) fluxes. Similarly, Fig. 3b, Fig. 4b and Fig. 5b show the SEM images recorded with zero flux (magnification 60 kx), NH_4Cl (magnification 65 kx), KNO_3 (magnification 67 kx) fluxes. The sample for zero flux has agglomeration, with particle size ~ 159 nm, after introducing flux, the number of voids increase for both fluxes shown in Fig. 4a and there

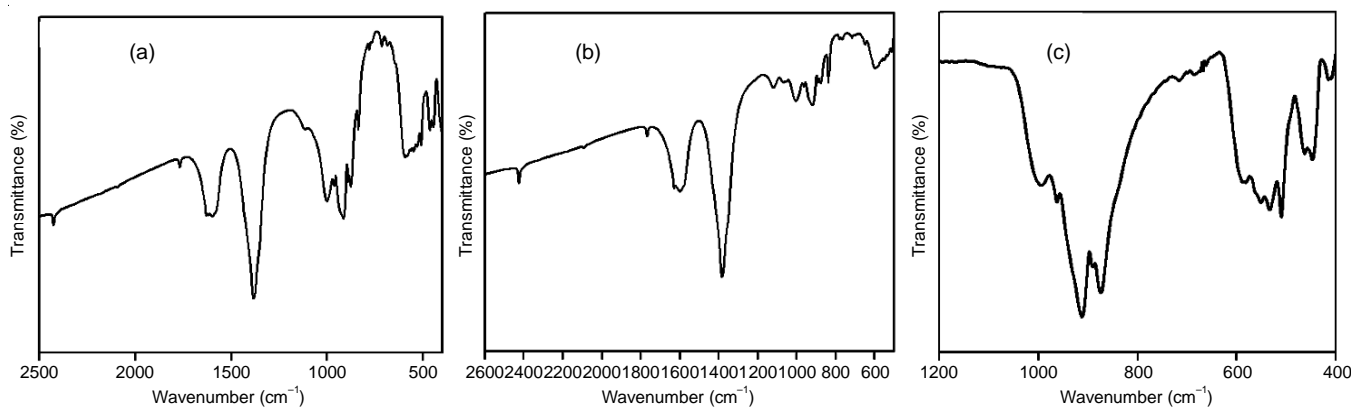


Fig. 2. FTIR spectra of the $Y_2SiO_5:Dy^{3+}$ (9 mol %) nanophosphors prepared using (a) zero flux, (b) NH_4Cl and (d) KNO_3 fluxes

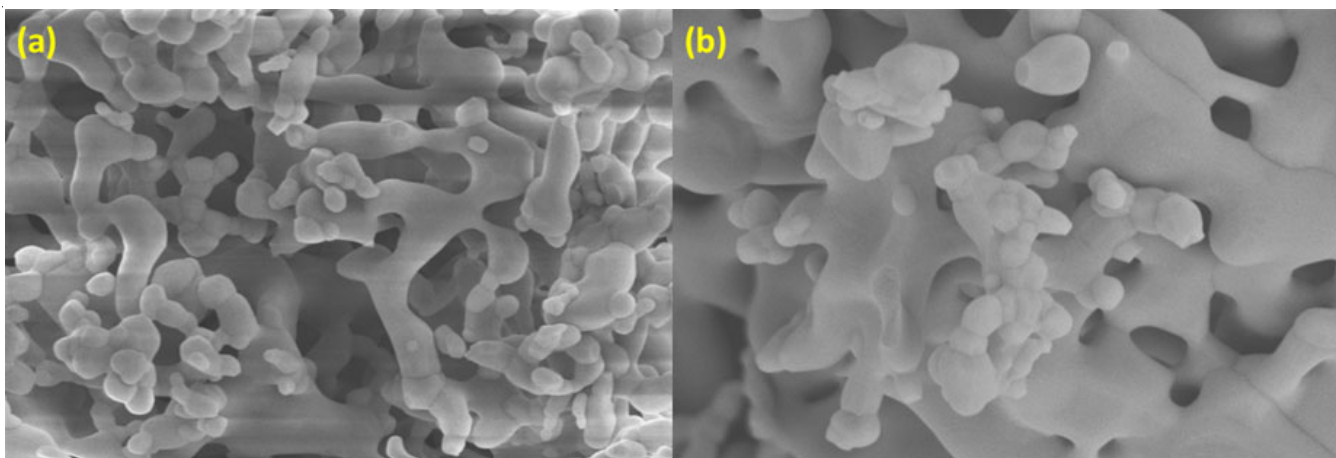


Fig. 3. SEM micrographs of zero flux, used in $Y_2SiO_5:Dy^{3+}$ (9 mol %) nanophosphors (magnification (a) 45 kx and (b) 60 kx)

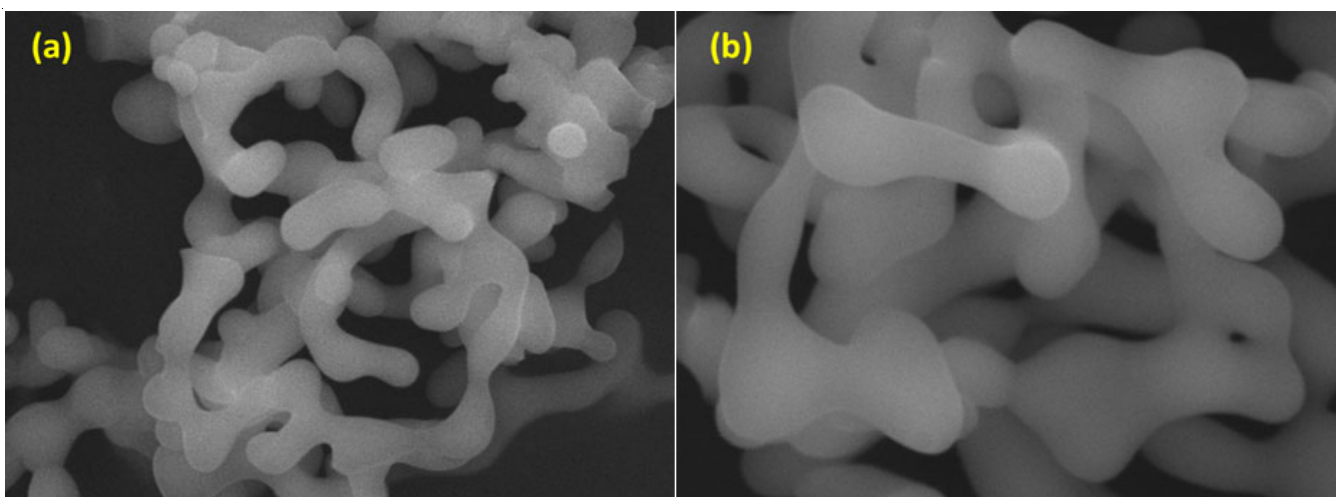


Fig. 4. SEM micrographs of $Y_2SiO_5:Dy^{3+}$ (9 mol %) nanophosphors with NH_4Cl flux (magnification (a) 40 kx (b) 65 kx)

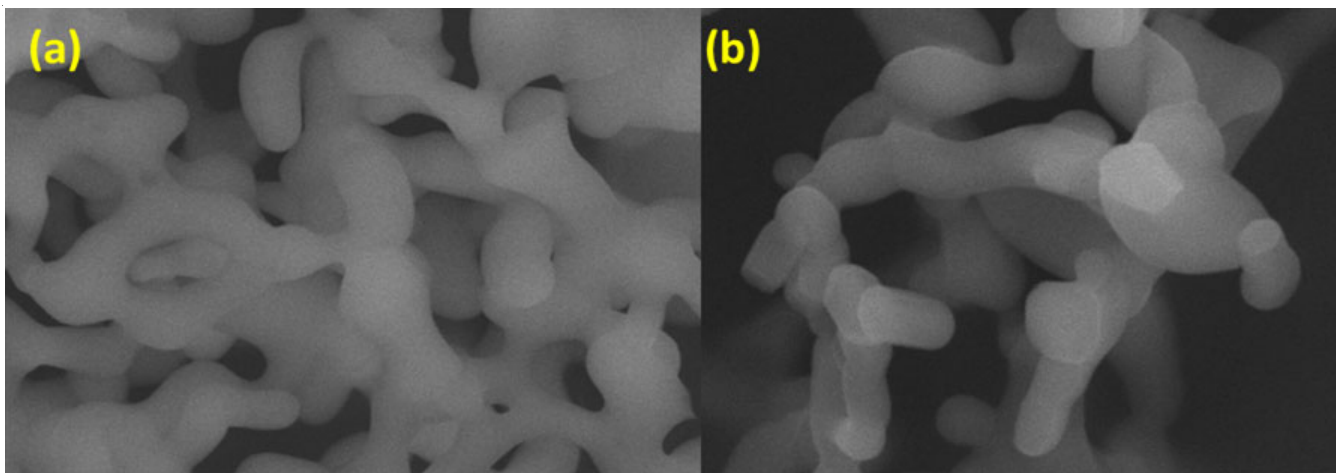


Fig. 5. SEM micrographs of $Y_2SiO_5:Dy^{3+}$ (9 mol %) nanophosphors with KNO_3 flux (magnification (a) 40 kx (b) 67 kx)

occurs enhanced grain growth with spherical shape shown in Fig. 4b and 5a, since the melting of flux can improve the slide and rotation of particles which can support particle-particle contact and particle growth [15,16].

While the melting point of NH_4Cl (338 °C) and KNO_3 (334 °C) fluxes is less than the solution combustion synthesis

reaction temperature (450 °C) this results in melting of flux components there by diffuses into the host reaction region.

In the calcining process, the melting of flux will eliminate the solid-solid grain boundaries and makes the particles to form a smooth surface [17,18]. Overall, by adding flux to the sample it attains smooth surface as shown in Fig. 4b and 5b.

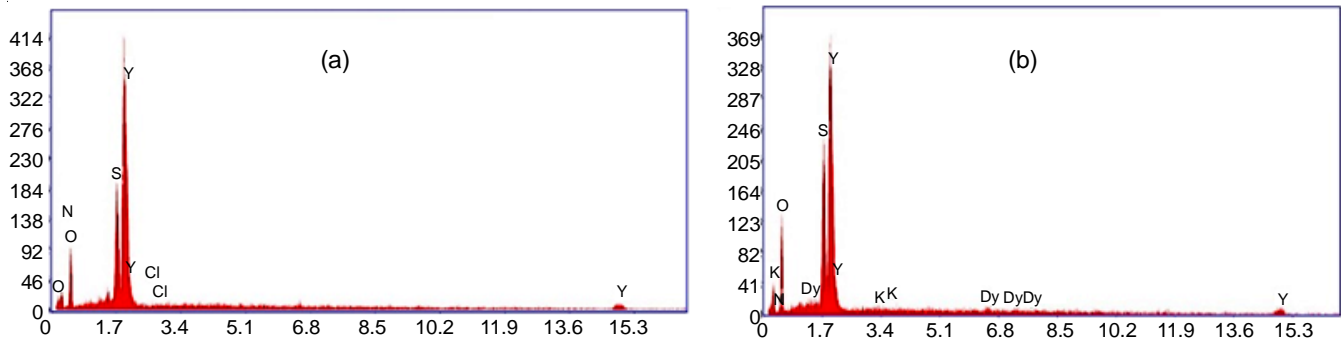


Fig. 6. EDAX patterns of (a) NH_4Cl and (b) KNO_3 used in $Y_2SiO_5:Dy^{3+}$ (9 mol %) nanophosphors

This improves the crystallinity and particle morphology of the sample. Further it effects the luminescence properties of the sample. The particle size distribution calculated is ~ 110 nm. To analyze the elements, present in the material elemental characterization of the phosphors was done by EDAX shown in Fig. 6. The atomic and weight % of the respective phosphors are shown in Table-1.

	Element	Weight (%)	Atomic (%)
(a)	N	5.82	11.90
	O	34.97	62.55
	Si	9.15	9.33
	Y	49.84	16.04
	Cl	0.22	0.18
(b)	N	3.27	6.51
	O	39.45	68.67
	Si	1.05	10.41
	Y	43.25	13.55
	K	0.48	0.34
	Dy	3.05	0.52

Thermoluminescence (TL) studies: Thermoluminescence glow curve for pure Y_2SiO_5 was observed around $205^\circ C$ and this can be referred in earlier publication [4]. Fig. 7 shows the $Y_2SiO_5:Dy^{3+}$ (9 mol%) nanophosphors with zero flux and NH_4Cl , irradiated with γ dose over a range of 500 Gy – 4 KGy at a constant heating rate $3^\circ C s^{-1}$. $Y_2SiO_5:Dy^{3+}$ (9 mol%) nanophosphor is the optimized sample as reported in our previous study [5]. The sample show prominent peak at $138^\circ C$ with a shoulder peak at $237^\circ C$ and a small hump at $180^\circ C$. These three peaks *i.e.* two glow peaks and a small hump signifies the presence of three kinds of trapping centers with γ -irradiation. At low temperature, the shallow trapping centers are responsible for the shoulder peaks, whereas the deeper center provides the glow peak at higher temperature side [19].

In present study, the effect of NH_4Cl and KNO_3 fluxes were analyzed on the TL intensity for $Y_2SiO_5:Dy^{3+}$ phosphors. From Fig. 7 (500 Gy–4 KGy), it is evident that there occur two peaks at $139^\circ C$ and at $210^\circ C$ for zero flux sample. The NH_4Cl doped phosphor exhibited a central TL glow peak shaped curve at around $138^\circ C$ and $237^\circ C$, which were matched with the previous report [19]. The shift in the peak *i.e.* (210 – $237^\circ C$) for before and after adding flux is due to the high

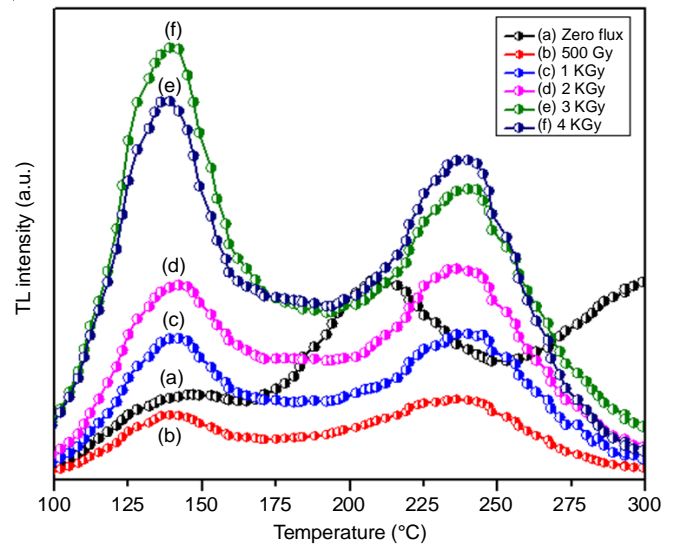


Fig. 7. Effect of γ -dose on TL glow curves of $Y_2SiO_5:Dy^{3+}$ (9 mol%) nanophosphor at a heating rate of $3^\circ C s^{-1}$ (a) zero flux, (b-f) NH_4Cl flux

lattice stability. Higher is the lattice stability higher temperature is the TL response which is interconverted to lattice stability.

The NH_4Cl doped sample shows the higher TL efficiency than the zero-flux sample. This high TL efficiency is mainly due to the large number of charge carriers and trapping centers which are highly efficient for the structural and morphological defects of the sample. Hence, it is inferred that a greater number of defects stronger the TL response. This could be the probable reason for the high TL in NH_4Cl doped sample [20].

Furthermore, there exists a linear increase of intensity of TL glow curves with γ -dose for the shoulder peak as well as prominent peak shown in Fig. 8. High TL intensity can be described based on the track interaction model [21]. As per this model, the number of traps created by the high energy radiation depend on the length of the track and cross-section inside the matrix. With increase in dose TL intensity also increases as few particles survive which may be lost while intended by high γ -dose due to small size of the particle. This linear pattern is very useful for dosimetric applications [22].

Furthermore, the dose response can be either, linear, sub-linear or super linear based on the linearity indexes [23] given by the equation:

$$TL = a (\text{Dose})^b \quad (2)$$

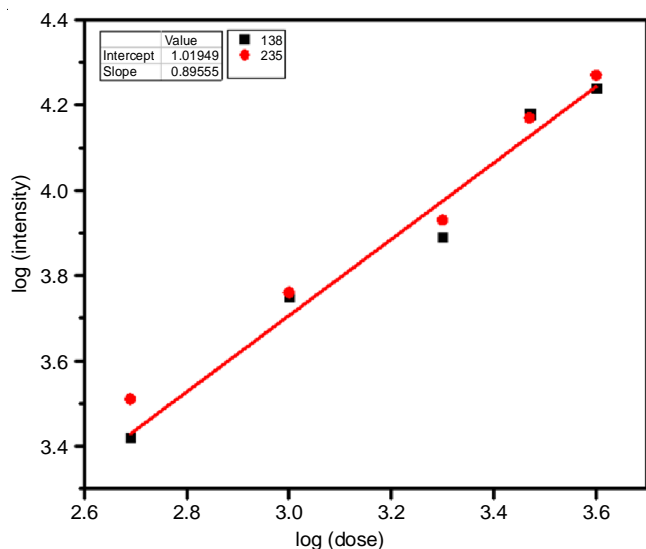


Fig. 8. Linear behaviour for various γ -doses of $Y_2SiO_5:Dy_x^{3+}$ doped with flux1 nanophosphor

Doing logarithms on either side of the equation:

$$\text{Log TL} = \text{log a} + \text{b log (dose)} \quad (3)$$

where 'a' denotes constant and the slope ($b = \text{linear factor}$) is obtained by linear fit of log TL versus log dose . If $b = 1$ dose response is linear, whereas sub-linear if $b < 1$ and if $b > 1$ it is super linear. In present work, the approximate 'b' value was found to be 0.89 (< 1), as shown in Fig. 9, indicating the dose response is sub-linear.

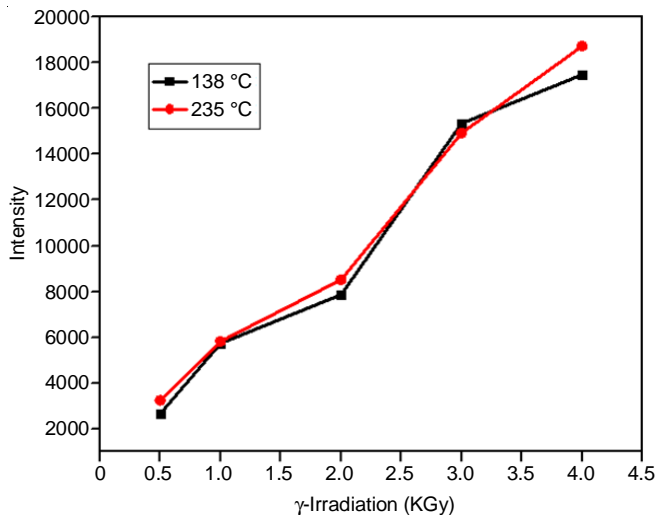


Fig. 9. Dose response of $Y_2SiO_5:Dy_x^{3+}$ (9 mol%) doped with NH_4Cl flux nanophosphor in log-log scale

Fig. 9 shows the plot between the maximum log TL intensity and log (dose) of $Y_2SiO_5:Dy_x^{3+}$ doped with NH_4Cl phosphor. Fig. 10 represents the de-convoluted plots of TL glow curves of $Y_2SiO_5:Dy_x^{3+}$ doped with NH_4Cl phosphor. Similarly, the TL glow curves of KNO_3 doped with $Y_2SiO_5:Dy_x^{3+}$ (9 mol%) phosphors with different doses are shown in Fig. 11. It is evident from the figure there exists a broad peak around 151 °C and hump around 200 °C for 500 Gy. On further increase in dose, the peak gradually sharpens and shifts slightly to lower temp-

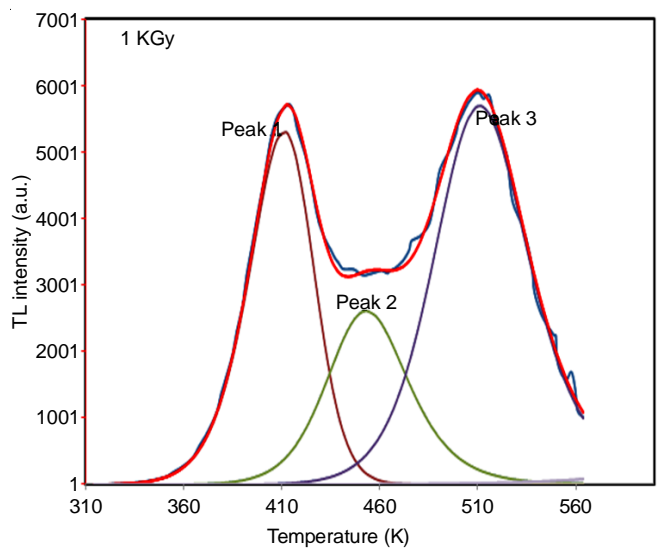


Fig. 10. Deconvolution of $Y_2SiO_5:Dy_x^{3+}$ (9 mol%) doped with NH_4Cl flux phosphor

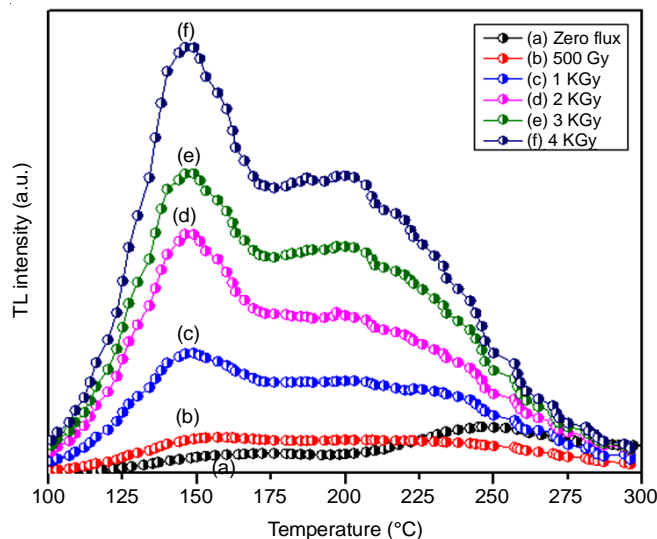


Fig. 11. Effect of γ -dose on TL glow curves of $Y_2SiO_5:Dy_x^{3+}$ (9 mol%) nanophosphor doped with KNO_3 flux at a heating rate of $3 \text{ }^\circ\text{C s}^{-1}$

erature around 145 °C remaining the hump as constant. This shift in the glow peak towards lower temperature and sharp increase are due to contribution of shallow trapping centers signifying for the betterment of large number of trap centers. According to the literature, the effect of KNO_3 gives rise to three TL glow peak curves around 385, 192 and 239 °C, which were in quite agreement with the present phosphors [24].

Moreover, the increase in intensity with respect to various dose of the phosphor were recorded as shown in Fig. 12 also calculated b value, which is $1.13 > 1$ indicating the dose response to be as super linear shown in Fig. 13. The graph indicates the linear behaviour. From the literature, it can be analyzed that the defect centers are produced in the oxides and affect energy transfer which reacts with the radical species of nitrate ions.

Discussion of trapping parameters: Usually, one or more peaks in the glow curves were observed by TL phosphors when charge carriers are released. The glow curve represents different trap levels which lie within the bandgap of the material. These

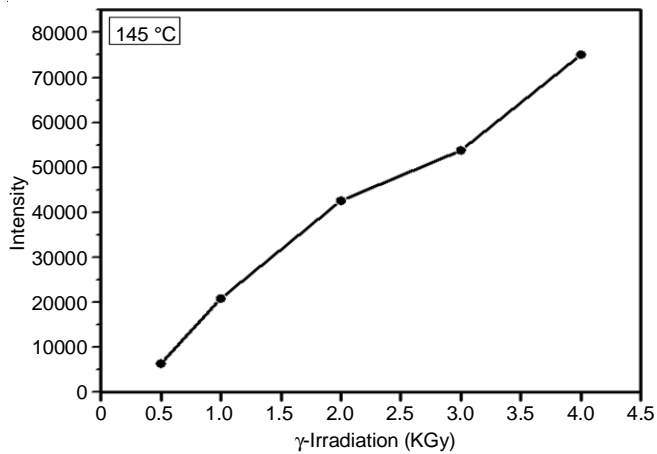


Fig. 12. Linear behaviour for various γ -doses of $Y_2SiO_5:Dy^{3+}$ (9 mol%) nanophosphor doped with KNO_3 flux

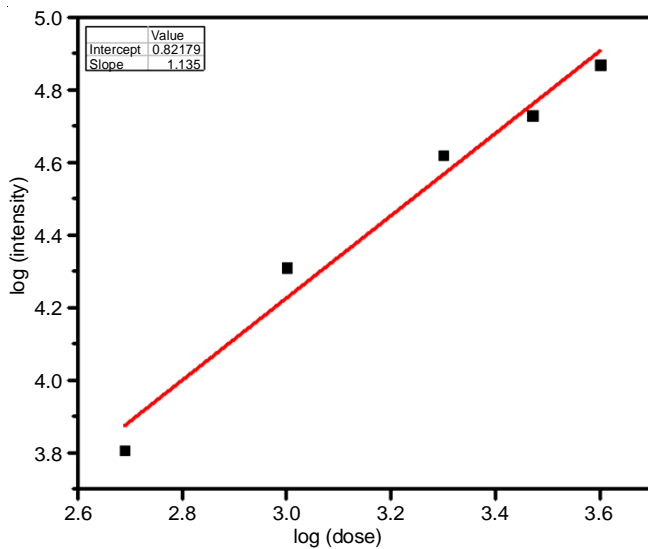


Fig. 13. Dose response of $Y_2SiO_5:Dy^{3+}$ (9 mol%) nanophosphor doped with KNO_3 flux in log-log scale

traps were described by specific parameters such as trap depth (E) and frequency factor (S).

Significant knowledge of these parameters is required for many TL applications [25-27]. The glow curve deconvolutions (GSD) were done for the TL glow peaks of the irradiated phosphors shown in Figs. 10 and 14 by using the Kittis & Gomez-Ros [28] to obtain first and second order kinetics. To identify the nature of traps formed in the samples under γ -irradiation we employed glow curve peak shape method adapted by various researches [29-33]. The TL glow curves for 1 KGY

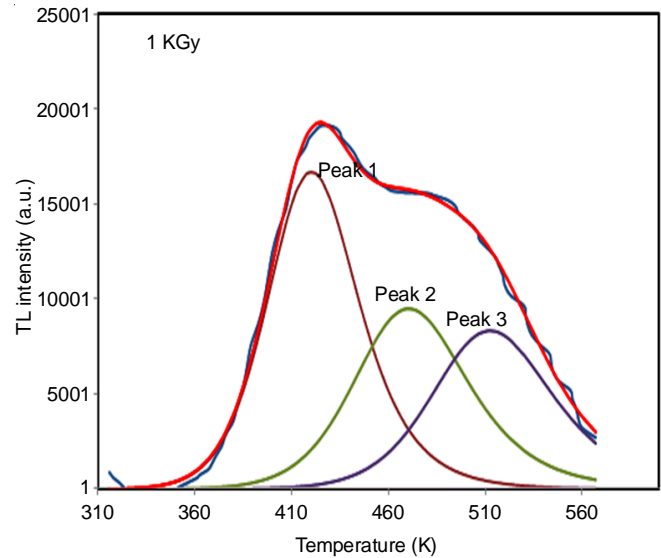


Fig. 14. Deconvolution of $Y_2SiO_5:Dy^{3+}$ (9 mol%) nanophosphors doped with KNO_3 flux

γ -dose for all the different flux are analyzed based on the glow curve peak shape method adapted by Chen [33].

Kinetic parameters were estimated using eqns. 4-6:

$$E_{\alpha} = C_{\alpha} \left(\frac{KT^2 m}{\infty} \right) - b_{\alpha} (2kT_m) \quad (4)$$

where $\alpha = \tau, \delta$ and ω with $\tau = T_m - T_1$, $\delta = T_2 - T_m$ and $\omega = T_2 - T_1$

$$C_{\tau} = 1.51 + 3.0 (\mu_g - 0.42), b_{\tau} = 1.58 + 4.2(\mu_g - 0.42)$$

$$C_{\delta} = 0.976 + 7.3 (\mu_g - 0.42), b_{\delta} = 0$$

$$C_{\omega} = 2.52 + 10.2 (\mu_g - 0.42), b_{\omega} = 1$$

The form factor (symmetry factor; μ_g) is given by:

$$\mu_g = \frac{\delta}{\omega} = \frac{T_2 - T_m}{T_2 - T_1} \quad (5)$$

$$\frac{\beta E}{KT_m^2} = S \exp \left\{ \frac{-E}{kT_m^2} \right\} [1 + (b-1)\Delta_m] \quad (6)$$

where $\Delta = 2kT/E$ and $\Delta_m = 2kT_m/E$ and β represents linear heating rate and K stands for Boltzmann constant (8.6×10^{-5} eV K^{-1}), (s) = frequency factor and (b) = order of the kinetics. Table-2 illustrates the list trapping parameters for various fluxes. Activation energy is the energy needed to remove the trapped charge carriers from the/defect center to the conduction band. The glow curve deconvolution was used to analyze the activation energy which is part of the kinetic parameters. This energy (E) value lies between 1.01-1.3 for NH_4Cl and for KNO_3

TABLE-2
ESTIMATED KINETIC PARAMETERS OF $Y_2SiO_5:Dy^{3+}$ (9 mol%) NANOPHOSPHOR DOPED WITH DIFFERENT FLUXES

Flux	Peak	T_1	T_2	T_m ($^{\circ}C$)	ω	$b(\mu_g)$	E_{avg}	Frequency factor, S (s^{-1})
NH_4Cl	1	390	429	411	39.10	1 (0.45)	1.02	8.22×10^{11}
	2	429	478	453	49.03	2 (0.52)	1.01	7.15×10^{12}
	3	483	541	511	57.47	2 (0.52)	1.30	1.80×10^{12}
KNO_3	1	393	449	420	55.53	2 (0.52)	0.90	1.73×10^{10}
	2	437	506	470	68.95	2 (0.52)	0.90	9.74×10^8
	3	477	550	512	73.21	2 (0.52)	1.01	1.80×10^9

varies from 0.9-1.01. Order of kinetics (b) can be expected from the symmetry factor (μ_g) of the glow peak from eqn. 5 by knowing δ and ω . The μ_g value lies between 0.42-0.52. Here for NH_4Cl except for one peak the other two peaks have 0.52 signifying second order. Similarly, for KNO_3 μ_g value is found to be 0.52 indicating second order. Hence, the thermal curves of the flux follow second order kinetics. After resolving order of kinetics frequency factor (S) is estimated by using eqn. 6.

It can be concluded that maximum peaks followed second order kinetics signifying the occurrence of retrapping phenomena. All these properties inferred that the phosphors were best suitable for dosimetry applications.

Conclusion

To improve the luminescence properties of prepared $\text{Y}_2\text{SiO}_5:\text{Dy}^{3+}$ (9 mol%) nanophosphors were doped with NH_4Cl and KNO_3 fluxes. It was observed that effect of flux influences the host by broadening of the peaks and hence it results small crystallite size \sim 20-22 nm. By incorporating flux, effect on stretching of bonds occurred which is revealed by FTIR data. In thermoluminescence (TL) studies, adding flux take the lead of shifting of peak towards lower temperature and sharp increase in peak. This in turn leads to creation of several kinds of trapping centers signifying high thermoluminescence efficiency than zero flux. The linear response of doped flux was found to be super linear on comparison with zero flux. This super linear behaviour is highly useful for the dosimetry applications. Activation energy was calculated for doped flux, which implies that different trap depths are located enclosed by the bandgap of phosphor.

CONFLICT OF INTEREST

The authors declare that there is no conflict of interests regarding the publication of this article.

REFERENCES

- A.R. Kadam, G.C. Mishra and S.J. Dhoble, *J. Mol. Struct.*, **1225**, 129129 (2021); <https://doi.org/10.1016/j.molstruc.2020.129129>
- G. Kitis and V. Pagonis, *Detect. Assoc. Equip.*, **913**, 78 (2019); <https://doi.org/10.1016/j.nima.2018.10.056>
- W.Y. Ching, L. Ouyang and Y.-N. Xu, *Phys. Rev. B*, **67**, 245108 (2003); <https://doi.org/10.1103/PhysRevB.67.245108>
- K. Dhanalakshmi, A.J. Reddy, D.L. Monika, R. Hari Krishna and L. Parashuram, *J. Non-Cryst. Solids*, **471**, 195 (2017); <https://doi.org/10.1016/j.jnoncrysol.2017.05.040>
- K. Dhanalakshmi, R.H. Krishna, A.J. Reddy, M.N. Chandraprabha, D.L. Monika and L. Parashuram, *Appl. Phys., A Mater. Sci. Process.*, **125**, 526 (2019); <https://doi.org/10.1007/s00339-019-2814-3>
- K. Dhanalakshmi, A.J. Reddy and L. Parashuram, *Asian J. Chem.*, **31**, 917 (2019); <https://doi.org/10.14233/ajchem.2019.21850>
- Y. Parganiha, J. Kaur, V. Dubey and D. Chandrakar, *Superlattices Microstruct.*, **77**, 152 (2015); <https://doi.org/10.1016/j.spmi.2014.11.010>
- H.T. Haile and F.B. Dejene, *Inorg. Chem. Commun.*, **127**, 108554 (2021); <https://doi.org/10.1016/j.inoche.2021.108554>
- M.M. Gowri, G.P. Darshan, Y.V. Naik, H.B. Premkumar, D. Kavyashree, S.C. Sharma and H. Nagabhushana, *Opt. Mater.*, **96**, 109282 (2019); <https://doi.org/10.1016/j.optmat.2019.109282>
- G. Ramakrishna, H. Nagabhushana, D.V. Sunitha, S.C. Prashantha, S.C. Sharma and B.M. Nagabhushana, *Spectrochim. Acta A Mol. Biomol. Spectrosc.*, **127**, 177 (2014); <https://doi.org/10.1016/j.saa.2014.02.054>
- T. Manohar, S.C. Prashantha, H.P. Nagaswarupa, R. Naik, H. Nagabhushana, K.S. Anantharaju, K.R.V. Mahesh and H.B. Premkumar, *J. Lumin.*, **190**, 279 (2017); <https://doi.org/10.1016/j.jlumin.2017.05.070>
- L. Liu, R.-J. Xie, C. Zhang and N. Hirotsaki, *Materials*, **6**, 2862 (2013); <https://doi.org/10.3390/ma6072862>
- A.J. Reddy, M.K. Kokila, H. Nagabhushana, S.C. Sharma, J.L. Rao, C. Shivakumara, B.M. Nagabhushana and R.P.S. Chakradhar, *Mater. Chem. Phys.*, **133**, 876 (2012); <https://doi.org/10.1016/j.matchemphys.2012.01.111>
- X.M. Han, J. Lin, J. Fu, R.B. Xing, M. Yu, Y.H. Zhou and M.L. Pang, *Solid. State. Sci.*, **6**, 349 (2004); <https://doi.org/10.1016/j.solidstatesciences.2004.02.004>
- W. Wang, B. Liu, Y. Wang, Z. Zhang, Y. Chen and L. Wei, *Mater. Lett.*, **65**, 3580 (2011); <https://doi.org/10.1016/j.matlet.2011.07.080>
- T.T. Lai, C.C. Chang, C.Y. Yang, S. Das and C.H. Lu, *Ceram. Int.*, **39**, 159 (2013); <https://doi.org/10.1016/j.ceramint.2012.06.004>
- Y. Yu, H. Wang, L. Li, Y. Chen and R. Zeng, *Ceram. Int.*, **40**, 14171 (2014); <https://doi.org/10.1016/j.ceramint.2014.06.004>
- J.L. Qin, H.R. Zhang, B.F. Lei, C.F. Hu, J.F. Li, Y.L. Liu, J.X. Meng, J. Wang, M.T. Zheng and Y. Xiao, *J. Am. Ceram. Soc.*, **96**, 3149 (2013); <https://doi.org/10.1111/jace.12471>
- Y.S. Vidya and B.N. Lakshminarasappa, *Appl. Phys., A Mater. Sci. Process.*, **118**, 249 (2015); <https://doi.org/10.1007/s00339-014-8669-8>
- M. Barboza-Flores, S. Gastélum, E. Cruz-Zaragoza, R. Meléndrez, V. Chernov, M. Pedroza-Montero and A. Favalli, *Radiat. Meas.*, **43**, 379 (2008); <https://doi.org/10.1016/j.radmeas.2007.11.055>
- Y.S. Horowitz, M. Rosenkrantz, S. Mahajana, D. Yosian, *J. Phys. D. Appl. Phys.*, **29**, 205 (1996); <https://doi.org/10.1088/0022-3727/29/1/031>
- B.S. Ravikumar, H. Nagabhushana, S.C. Sharma, Y.S. Vidya and K.S. Anantharaju, *Spectrochim. Acta A Mol. Biomol. Spectrosc.*, **136**, 1027 (2015); <https://doi.org/10.1016/j.saa.2014.09.126>
- C. Furetta, *Handbook of Thermoluminescence*, World Scientific, Singapore, Ed.: 2 (2003).
- G.A.T. Duller and L. Bøtter-Jensen, *Radiat. Prot. Dosimetry*, **47**, 683 (1993); <https://doi.org/10.1093/oxfordjournals.rpd.a081832>
- A.J.J. Bos, *Nucl. Instrum. Methods B*, **184**, 3 (2001); [https://doi.org/10.1016/S0168-583X\(01\)00717-0](https://doi.org/10.1016/S0168-583X(01)00717-0)
- G. Kitis, C. Furetta, M. Prokic and V. Prokic, *J. Phys. D Appl. Phys.*, **33**, 1252 (2000); <https://doi.org/10.1088/0022-3727/33/11/302>
- B.A. Sharma, A.N. Singh, S.N. Singh and O.B. Singh, *Radiat. Meas.*, **44**, 32 (2009); <https://doi.org/10.1016/j.radmeas.2008.06.001>
- G. Kitis and J.M. Gomez-Ros, *Nucl. Instrum. Methods Phys. Res. A*, **440**, 224 (2000); [https://doi.org/10.1016/S0168-9002\(99\)00876-1](https://doi.org/10.1016/S0168-9002(99)00876-1)
- R. Tiwari, P. Bala Taunk, R. Kumar Tamarkar, N. Kumar Swamy and V. Dubey, *Chalcogenide Lett.*, **11**, 141 (2014).
- R.K. Tamrakar and D.P. Bisen, *Res. Chem. Intermed.*, **39**, 3043 (2013); <https://doi.org/10.1007/s11164-012-0816-2>
- S. Mahajna and Y.S. Horowitz, *J. Phys. D Appl. Phys.*, **30**, 2603 (1997); <https://doi.org/10.1088/0022-3727/30/18/016>
- Y.S. Horowitz, O. Avila and M. Rodriguez-Villafuerte, *Nucl. Instrum. Methods B*, **184**, 85 (2001); [https://doi.org/10.1016/S0168-583X\(01\)00710-8](https://doi.org/10.1016/S0168-583X(01)00710-8)
- R. Chen, *J. Electrochem. Soc.*, **116**, 1254 (1969); <https://doi.org/10.1149/1.2412291>